Automatic identification of the plasma equilibrium operating space in tokamaks

Xiao Song, Eric Nardon, Holger Heumann, Blaise Faugeras

Automatic identification of the plasma equilibrium operating space in tokamaks☆

X.Song[a,c,*], E.Nardon[b], H.Heumann[c], B.Faugeras[c]

[a] *Southwestern Institute of Physics, P.O.Box 432, Chengdu, 610041, China*
[b] *CEA, IRFM, F-13108 Saint-Paul-lez-Durance, France*
[c] *Team CASTOR, INRIA, Laboratoire J.A. Dieudonné, CNRS UMR 7351, Université Côte d'Azur, France*

Abstract

In order to identify the plasma equilibrium operating space for future tokamaks, a new *objective* function is introduced in the inverse static free-boundary equilibrium code FEEQS.M. This function comprises terms which penalize the violation of the central solenoid and poloidal field coils limitations (currents and forces). The penalization terms do not require any weight tuning. Hence, this new approach automatizes to a large extent the identification of the operating space. As an illustration, the new method is applied on the ITER 15 and 17 MA inductive scenarios, and similar operating spaces compared to previous works are found. These operating spaces are obtained within a few (~ 3) hours of computing time on a single standard CPU.

Keywords: `plasma equilibrium,inverse static,objective function,ITER scenario`

1. Introduction

In a tokamak, the central solenoid (CS) and poloidal field (PF) coils always have limitations in the current they can carry, the force they can handle and, for superconducting coils, the magnetic field they can tolerate. It is clear that these limitations will translate into restrictions on the accessible domain of plasma equilibria, but it is not easy for a human to determine exactly what these restrictions will be. The plasma equilibrium domain in the general sense is defined by the set of possible plasma shape, plasma current, flux state (Ψ_{st}) and internal profiles (β_p and $l_i(3)$), where Ψ_{st} is the poloidal flux [1] from all the contributions of the CS and PF currents in a specified position inside the plasma area. In this paper, we consider a given plasma shape, plasma current and plasma β_p, and look at a cross-section of the multi-dimensional plasma equilibrium domain in the $l_i(3)$-Ψ_{st} plane [2]. Such $l_i(3)$-Ψ_{st} diagrams are useful for inductive scenarios, in which the plasma current and shape are established for a long duration while Ψ_{st} is varied in time and $l_i(3)$ may also change due, e.g. to a L-H transition.

A number of equilibrium codes have been used in the past to identify the ITER 15 and 17 MA operating spaces in $l_i(3)$-Ψ_{st} domain, which led to modifications in the ITER design in order to extend this space [3]. These codes are typically inverse static free-boundary equilibrium (FBE) solvers, which find a set of CS and PF coils currents by minimizing an *objective* function which comprises two terms: the first one, which is called here the *cost function*, quantifies the distance between the computed and desired plasma shape; the second one is a *regularization* term, which is usually a weighted sum of the squares of the CS and PF coils currents. With this *objective* function, the real limits are not taken into account. One possible solution to this issue is to carefully tune the weights until all the limits are respected, but this requires much experience and can be a time-consuming task. Another possibility, as done in [4], is to linearize the FBE problem and to express all the limits as inequalities on the coils currents.

In this paper, we propose another solution, which is more general: we keep the non-linear FBE problem and we introduce a new *objective* function which accounts for the true limits with the non-linear constraints. The latter is based on penalization terms which increase sharply when one limit is overcome. Thanks to this approach, operating space diagrams may be obtained without needing to tune any weight. As an example, the new approach is applied to the ITER 15 and 17 MA inductive scenarios. The obtained $l_i(3)$-Ψ_{st} diagrams are similar to those found by previous works [2, 3, 4]. Each diagram is produced within a single run which takes ~ 3 hours on a standard computer.

The paper is organized as follows: section 2 introduces the mathematical formulation of the problem, including the new objective function; then section 3 presents the results for the ITER 15 and 17 MA operating space; section 4 is the conclusion.

2. Mathematical formulation

In this paper, we use the inverse static solver of the FEEQS.M FBE code [5], which finds CS and PF coils cur-

*corresponding author
Email address: `songx@swip.ac.cn` (X.Song)

rents that minimize the new *objective* function subject to the FBE equation. The equations of the static inverse FBE problem will be introduced in the section 2.1, and the *objective* function will be detailed in section 2.2.

2.1. The inverse static equilibrium problem

From the plasma force balance equation and Maxwell's equations, one can get the Grad-Shafranov equation [6]:

$$\begin{aligned} \Delta^*\psi &= rp'(\psi) + \frac{1}{\mu_0 r} ff'(\psi) \\ \Delta^*\psi &= -\nabla \cdot \left(\frac{1}{\mu r} \nabla \psi \right) = j_\phi \end{aligned} \tag{1}$$

where ψ is the poloidal flux, j_ϕ is the toroidal current density, p is plasma kinetic pressure, f is the diamagnetic function. The $p'(\psi)$ and $ff'(\psi)$ are parameterized in this paper as:

$$\begin{aligned} p'(\psi) &= \frac{\beta}{R_0}(1-\psi_N^\alpha)^\gamma \\ ff'(\psi) &= (1-\beta)\mu_0 R_0 (1-\psi_N^\alpha)^\gamma \end{aligned} \tag{2}$$

where $\psi_N = (\psi - \psi_{ax})/(\psi_{bd} - \psi_{ax})$ is the poloidal flux normalized so as to be 0 on the magnetic axis and 1 at the plasma boundary. R_0 is the major radius of vacuum vessel. A pedestal is not considered here for simplicity, but it is still important to explore the influence of the pedestal on the equilibrium operating space in future work.

In the CS and PF coils, we have: $j_\phi = I/S$, where I is the coil current, S is the area of the poloidal cross-section of the coil. Based on the fact that the induced loop voltage is small in the flat-top phase, the induced currents in the passive conducting structures are neglected here.

Thus, the FBE problem can be written as:

$$\Delta^*\psi = \begin{cases} rp'(\psi) + \dfrac{1}{\mu_0 r} ff'(\psi) & \text{in the plasma} \\ \dfrac{I_i}{S_i} & \text{in coil number } i \\ 0 & \text{elsewhere} \end{cases} \tag{3}$$

complemented by the following boundary conditions:

$$\begin{aligned} \psi(0,z) &= 0, \\ \lim_{\|(r,z)\| \to +\infty} \psi(r,z) &= 0 \end{aligned} \tag{4}$$

The inverse static FBE problem consists in finding a set of I_i which minimizes a given function $\mathbf{objective}(\psi, I_i)$ under the constraint of Eqs. (3)(4).

2.2. The new objective function

The new *objective* function is composed of two *cost function* terms (denoted with a C) and two penalization terms (denoted with a P):

$$\mathbf{objective} = \mathbf{C_{Shape}} + \mathbf{C_{Flux}} + \mathbf{P_{Current}} + \mathbf{P_{Force}} \tag{5}$$

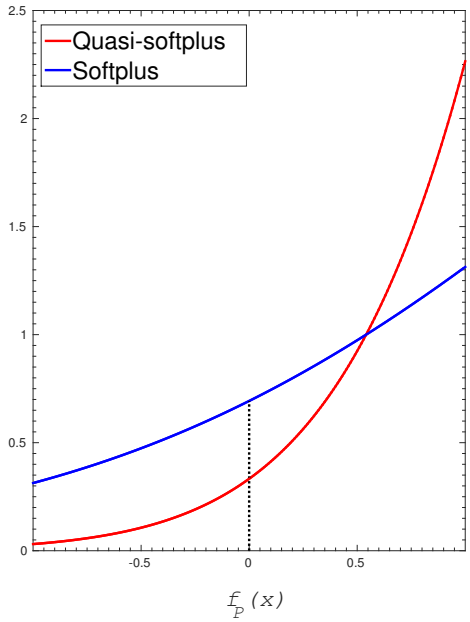

Figure 1: The penalization function of *quasi-softplus* f_P and the general *softplus* , where $x = 0$ represents the limit value for the current or force.

The first term,

$$\mathbf{C_{Shape}}(\psi) = \frac{1}{2} \sum_{i=1}^{N} (\psi(r_i, z_i) - \psi(r_0, z_0))^2 \tag{6}$$

tends to make all points (r_i, z_i), which describe the target separatrix, belong to the same flux surface. This kind of term is common in the literature. However, it may be remarked that $\mathbf{C_{Shape}}$ does not directly quantify the physical distance between the actual and the target separatrices. As a consequence, it is not possible to implement tolerances for this distance in the *cost function*. In the present work, we check these tolerances in post-processing, as detailed below in Fig. 2. Being able to directly impose tolerances through the *cost function* would however be of high practical value, and is a direction for future work.

The second term,

$$\mathbf{C_{Flux}}(I_{coils}) = \frac{1}{2} \left(M \cdot I_{coils} - \Psi_{st} \right)^2 \tag{7}$$

aims at matching the desired value of the flux state Ψ_{st}. Here M is the mutual inductance between the CS or PF coils and a toroidal wire at center of the vacuum vessel.

The third and fourth terms penalize respectively the violation of limits on the coils currents and coils forces. Here a penalization term is not used for the limits on the coils magnetic fields for simplicity. Post-processing of the results presented below suggests that taking these limits into account would almost not change the operational domain.

The force penalization term concerns the volume integrated force which, due to axisymmetry, is vertical:

$$F_{Z,i} = 2\pi \frac{I_i}{S_i} \int \partial_z \psi \, dS \qquad 1 \leq i \leq N_{coils} \tag{8}$$

The penalization terms are based on the *softplus* function elevated to the cubic power, we call it *quasi-softplus*:

$$\text{Quasi-softplus:} \qquad f_P(x) = (\text{softplus})^3 = \ln^3(1+e^x) \tag{9}$$

which is represented in Fig. 1. This way, penalization terms are always active but rather small when all quantities are within the limits, and grow sharply when a limit is violated. The penalization terms are:

$$\begin{aligned} \mathbf{P_{Force}}(I_{coils}, \psi) = & \sum_{i=1}^{N_{coils}} f_P\left(\frac{F_{z,i} - F_{max,i}}{|F_{max,i}|}\right) \\ & + f_P\left(\frac{F_{min,i} - F_{z,i}}{|F_{min,i}|}\right) \\ \mathbf{P_{Current}}(I_{coils}) = & \sum_{i=1}^{N_{coils}} f_P\left(\frac{I_i - I_{max,i}}{|I_{max,i}|}\right) \\ & + f_P\left(\frac{I_{min,i} - I_i}{|I_{min,i}|}\right) \end{aligned} \tag{10}$$

Here F_{max} (resp. F_{min}) and I_{max} (resp. I_{min}) represent the upper (resp. lower) limits of force and current, respectively.

The *regularization* term used in previous works [2, 3, 4] is not included in the new *objective* function. Indeed, this term appears not necessary anymore, since the term of $\mathbf{C_{Flux}}(I_{coils})$ already regularizes the problem.

It is worth noting that the new *objective* function does not contain any adjustable weight.

In FEEQS.M, the quasi-Newton method described in [5] is applied to find the solution of the non-linear static inverse FBE problem. The first and second derivatives of the *objective* function are used to find the direction and the step length of the iterations. The convergence condition is:

$$\frac{\|I_{k+1} - I_k\|^2}{\|I_{k+1}\|^2} + \frac{\|\psi_{k+1} - \psi_k\|^2}{\|\psi_{k+1}\|^2} \leqslant \epsilon_0 \tag{11}$$

3. ITER 15 MA and 17 MA equilibrium operating spaces

The new tool is applied to identify the ITER 15 and 17 MA inductive scenario operating spaces, and the results are analyzed to give some suggestions to enlarge the operating space in this section.

In order to find the equilibrium operating space, a series of static inverse FBE calculations are performed, scanning the parameter γ which appears in Eq. (2) and is a proxy for $l_i(3)$, as well as Ψ_{st}, so as to map the $l_i(3) - \Psi_{st}$ space. The parameters α and β are fixed to 1 and 0.65, respectively, since $\beta_p = 0.6$ is the nominal value in the flat top phase for ITER cases. Our simulation results are weakly sensitive to α and β, consistently with the weak sensitivity to β_N reported in [3]. The operating space can then be visualized by plotting the iso-lines of the currents, fields and forces, as well as of the boundary deviation metric (gaps) in $l_i(3) - \Psi_{st}$ diagram. Note that $l_i(3)$ is calculated in the converged ψ map as:

$$l_i(3) = \frac{2\int B_\theta^2 dV}{(\mu_0 I_p)^2 R_0} \tag{12}$$

where B_θ is the poloidal magnetic field,and V is the plasma volume.

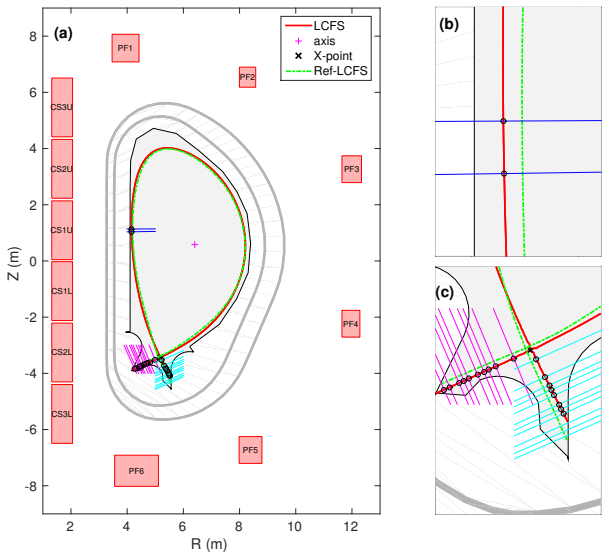

Figure 2: The poloidal geometry of ITER (a) and the definition of the separatrix deviation; (b) and (c) show close ups of the midplane high field side region and divertor region respectively. The blue, magenta and cyan lines show directions along which the distance between the desired (red) and actual (green) boundaries is calculated. This distance is then used to define the boundary deviation metrics. The description of 'dn' in Fig.3 and 4 means the actual divertor leg (red plain line) is below the reference (green dashed line).

Fig. 2 (a) shows the ITER reference separatrix and the poloidal field coils. Directions along with the gaps between the reference boundary and the actual one are also shown in Fig. 2 (b) and (c). The limitations of all the currents, fields and forces on the CS and PF coils as well as on boundary deviation limits for ITER scenarios are defined in [7].

Fig. 3 is the ITER 15 MA equilibrium operating space. The lines are iso-contours of the most critical current and field in coils, as well as of boundary deviation metrics. The iso-contour corresponding to the limit value for each quantity is shown in dashed bold. Plain thin lines are beyond the limit. The operation domain is therefore the zone left in white. It can be seen that for the ITER 15 MA

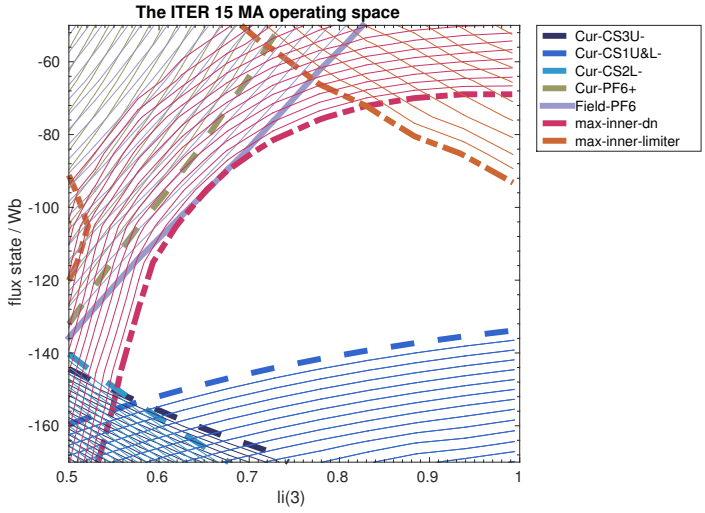

Figure 3: ITER inductive 15 MA operational space obtained with FEEQS.M, see text for a description. The symbol of '-' in the legend represents the lower limit and '+' is the upper limit, e.g. the 'Cur-CS1U&L-' represents the lower current limit of 'Cur-CS1U&L' coil is -45 kA/turn.

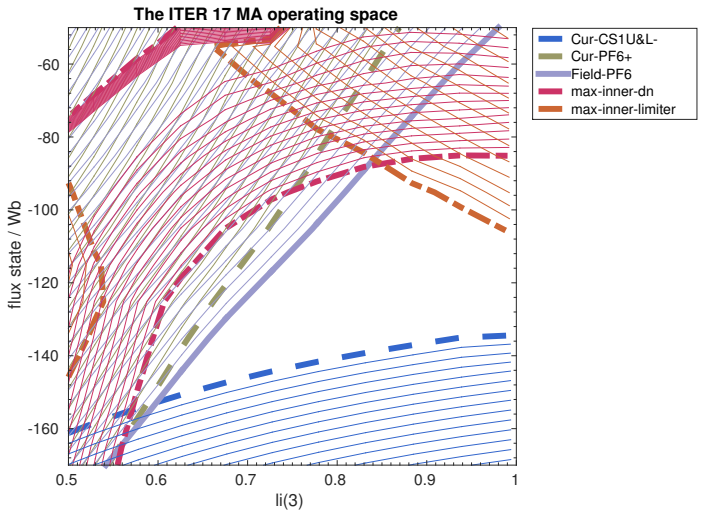

Figure 4: ITER inductive 17 MA operational space obtained with FEEQS.M, see text for a description.

case, in the high $l_i(3)$-$|\Psi_{st}|$ area the operating domain is constrained by the CS1U&L current, which seems logical since the main flux source is the CS coils. On the other hand, in the low $l_i(3)$ - $|\Psi_{st}|$ area, the operating bounds are determined by the maximum boundary tolerance, in the inner divertor leg region, nearly followed by the PF6 field and current. This seems again conform to the intuition since the PF6 coil provides the dominant magnetic field to control the divertor geometry. Finally, in the high $l_i(3)$ low $|\Psi_{st}|$ area the operating space is bounded by the inner limiter gaps, which is less easy to understand intuitively than the previous limits but may be related to a difficulty to control the CS stray field at low $|\Psi_{st}|$.

Fig. 4 gives the ITER 17 MA equilibrium operating space. It has a similar CS1U&L limitation at high $|\Psi_{st}|$ to the 15 MA case. The difference is that in the 17 MA case, the limitations of the PF6 current and field make the whole area smaller, because more PF6 current is needed when the plasma current is increased.

Overall, the operational domains identified by FEEQS.M appear quantitatively rather similar to Fig. 5 in [3] and Fig. 2 in [2]. In particular the currents limits in CS1U&L and field limits in PF6 for the 15 MA case are close to those shown in Fig. 5 of [3]. One difference is however visible in the top right corner of the domain where our simulations indicate a limitation due to the maximum distance between the wall and plasma on the inner side, which is not visible in [2, 3]. The reason for this difference is a subject for further study. The total computation time to obtain the 15 and 17 MA operating spaces above is around 3 hours in each case on a single standard CPU. It has not been necessary to tune any weight in order to produce Fig. 3 and Fig. 4. We believe that this important observation may be partly explained by the sharp growth of the penalization terms when the limits are violated.

4. Conclusion

An automatic way to identify the equilibrium operating space in tokamaks is achieved by applying a new *objective* function, which penalizes the violation of the CS and PF currents and force limitations, to constrain a series of inverse static FBE calculations.

The new method is utilized to find the ITER 15 and 17 MA equilibrium operating spaces, with similar results to previous works, but in a faster and much less human work intensive way.

With this new tool, evaluating the operating space for a new tokamak can be completed in a quick and accurate way.

Improvements could however still be made, e.g., as discussed above, in the *cost function* term which represents the deviation from the desired plasma boundary, or to include a pedestal in the plasma edge.

5. Acknowledgment

The views and opinions expressed herein do not necessarily reflect those of the ITER Organization. This work is supported by the Natural Science Foundation of China under Grant Nos 11805056.

References

[1] T. C. Luce, D. A. Humphreys, G. L. Jackson, W. M. Solomon, Inductive flux usage and its optimization in tokamak operation, Nuclear Fusion 54 (9) (2014) 093005.

[2] T. Casper, Y. Gribov, A. Kavin, V. Lukash, R. Khayrutdinov, H. Fujieda, C. Kessel, I. D. Agencies, et al., Development of the ITER baseline inductive scenario, Nuclear Fusion 54 (1) (2013) 013005.

[3] C. Kessel, D. Campbell, Y. Gribov, G. Saibene, G. Ambrosino, R. Budny, T. Casper, M. Cavinato, H. Fujieda, R. Hawryluk, et al., Development of ITER 15 MA ELMy H-mode inductive scenario, Nuclear Fusion 49 (8) (2009) 085034.

[4] M. Mattei, M. Cavinato, G. Saibene, A. Portone, R. Albanese, G. Ambrosino, L. Horton, C. Kessel, F. Koechl, P. Lomas, et al., ITER operational space for full plasma current H-mode operation, Fusion Engineering and Design 84 (2) (2009) 300–304.

[5] H. Heumann, J. Blum, C. Boulbe, B. Faugeras, G. Selig, J.-M. Ané, S. Brémond, V. Grandgirard, P. Hertout, E. Nardon, Quasi-static free-boundary equilibrium of toroidal plasma with CEDRES++: Computational methods and applications, Journal of Plasma Physics 81 (3).

[6] V. Mukhovatov, V. Shafranov, Plasma equilibrium in a tokamak, Nuclear Fusion 11 (6) (1971) 605.

[7] Y. Gribov, N. Mitchell, C. Jong, F. Simon, A. Loarte, CS and PF coils data and requirements to separatrix positioning for analysis of ITER plasma equilibria and poloidal field scenarios, ITER-D-2ACJT3, Version, 3.2 Edition (July 13, 2017).